Volume 01, Issue 01, October 2026

Journal of Sustainable Multidisciplinary Research (JSMR)
www.journalsmr.com | editor@journalsmr.com

Journal SMR

Energy-Aware Predefined-Time Formation Reconfiguration of Heterogeneous UAV Swarms via Gramian-Based Assignment and Safe Terminal Recovery

Vu Quang Luong[1]*, Trinh Thi Minh[2], Hoang Van Ngoi[1], Nguyen Duy Tien[1]

[1]*Missile Faculty, Air Defence-Air Force Academy, Hanoi, Vietnam*

[2]*Basic Sciences Faculty, Air Defence-Air Force Academy, Hanoi, Vietnam*

**Corresponding email: vuquangluong88@gmail.com*

DOI: https://doi.org/10.63680/JSMR092610.4

Keywords: control barrier function; energy-aware assignment; formation reconfiguration; minimum-energy control; predefined-time control; unmanned aerial vehicle swarm

Abstract

Predefined-time formation reconfiguration of unmanned aerial vehicle (UAV) swarms requires simultaneous satisfaction of a mission deadline, heterogeneous energy reserves, collision-separation constraints, actuator limits, and external disturbances. This study develops an energy-constrained predefined-time reconfiguration framework in which a single finite-horizon controllability Gramian is used consistently for both discrete slot assignment and continuous terminal recovery. The assignment stage minimizes a state-of-charge- and mass-weighted maneuver index while screening individual energy budgets and nominal pairwise separation. The online stage combines a receding minimum-energy terminal correction, effective-disturbance observation, and a high-order control-barrier-function safety projection. Under compound uncertainty, the method achieves a 0.00529 m formation-reference RMSE, a 0.00176 m deadline error, a 1.997 m minimum separation, and zero acceleration saturation. Relative to direct predefined-time mapping, reference maneuver effort decreases by 75.9%, tracking RMSE by 90.3%, and model-based incremental propulsion energy by 15.8%. Thirty paired common-seed trials retain 100% deadline success and consistent improvement over the strongest baseline. The results demonstrate that coupling deadline selection, energy-aware assignment, and receding terminal control through the same finite-horizon energy metric provides a compact and analytically interpretable solution for deadline-critical UAV-swarm reconfiguration.

1. Introduction

Formation-control research has progressed from static shape keeping to mission-driven assembly, reconfiguration, obstacle interaction, and coordinated task execution [1]. Predefined- and prescribed-time methods allow the convergence time to be selected explicitly and have been developed for UAV swarms and multi-agent systems under spatiotemporal constraints, directed graphs, switching topologies, uncertainty, disturbances, faults, and heterogeneous dynamics [2]-[19]. These advances address convergence-time specification effectively, but they do not by themselves resolve how a prescribed mission deadline should alter the energetic cost of assigning individual vehicles to target slots.

Formation reconfiguration is also naturally a coupled discrete-continuous problem. Target assignment and control-input optimization have been considered in two-stage and model-predictive frameworks [20], [21], while energy-aware cooperative control is increasingly important because multirotor endurance depends strongly on thrust, speed, acceleration, vehicle mass, and remaining battery charge [22]-[27]. A persistent gap is that deadline selection, heterogeneous energy reserve, slot assignment, and online terminal correction are usually treated as separate design layers. Consequently, the assignment may be energetically inefficient for the selected deadline, and the online controller may track a precomputed path without re-solving the finite-horizon steering problem from the current tracking error.

This work adopts an outer-loop translational model consistent with established UAV dynamics and disturbance-aware control practice [29]-[32], with the inner attitude dynamics assumed sufficiently faster than the formation layer. This separation enables

the deadline-energy relationship to be derived analytically and keeps the proposed architecture suitable for real-time swarm implementation.

Novelty. The central contribution is a unified deadline-energy co-design: the same finite-horizon controllability Gramian determines both the assignment cost before reconfiguration and the receding minimum-energy terminal correction during flight. This creates a direct analytical link between the user-selected completion time, heterogeneous vehicle energy reserve, discrete slot allocation, and online deadline recovery, which distinguishes the proposed framework from existing predefined/prescribed-time formation control [2]-[19], reconfiguration optimization [20], [21], and propulsion-energy evaluation [22]-[27].

The study makes three technical contributions: (i) a deadline-dependent slot-assignment criterion weighted by vehicle mass and state of charge and constrained by per-UAV maneuver budgets and nominal pairwise separation; (ii) a receding minimum-energy terminal correction integrated with effective-disturbance observation and high-order control-barrier safety, so deadline recoverability and collision avoidance are enforced within a common online control architecture; and (iii) a reproducible evaluation protocol comprising component ablation, paired Monte Carlo trials, and deadline-sensitivity analysis, which separates the contribution of assignment, disturbance rejection, terminal correction, and safety supervision.

2. Methodology and Algorithm Synthesis

2.1. Relative heterogeneous UAV model and problem statement

For follower i, let p_i and v_i denote the inertial position and velocity, respectively. The outer-loop acceleration command is u_i. A scalar b_i captures unknown control-effectiveness variation caused by mass/propulsion mismatch, while d_i contains wind and unmodeled acceleration. The model used by the formation layer is

$$\dot{p}_i = v_i, \qquad \dot{v}_i = \beta_i u_i + d_i - c_d(v_i - v_L), \quad i = 1,\ldots,N \tag{1}$$

where c_d is a small velocity-damping coefficient and (p_L, v_L) is the virtual-leader state. With the relative variables r_i = p_i - p_L and w_i = v_i - v_L,

$$r_i = p_i - p_L, \quad w_i = v_i - v_L, \quad \dot{r}_i = w_i, \quad \dot{w}_i = \beta_i u_i - a_L + d_i - c_d w_i \tag{2}$$

A shape switch starts at t_s. Each vehicle must be assigned exactly one target slot q_j and satisfy

$$r_i(t_s) = r_i^0, w_i(t_s) = w_i^0, r_i(t_s + T_p) = q_{\pi(i)}, w_i(t_s + T_p) = 0 \tag{3}$$

where the predefined maneuver duration T_p is selected before the maneuver and does not depend on the initial permutation.

2.2. Finite-horizon minimum-energy transfer

The first design question is the least squared-acceleration effort required to connect one vehicle to one candidate slot. For the relative double integrator,

$$J_{ij}(T_p) = \min_u \int_0^{T_p} \| u(\tau) \|_2^2 \, d\tau \tag{4}$$

Using

$$A = \begin{bmatrix} 0 & I \\ 0 & 0 \end{bmatrix}, \qquad B = \begin{bmatrix} 0 \\ I \end{bmatrix} \tag{5}$$

the finite-horizon controllability Gramian is

$$W(T)=\int_0^T e^{A\tau}BB^T e^{A^T\tau}d\tau=\begin{bmatrix} T^3I/3 & T^2I/2 \\ T^2I/2 & TI \end{bmatrix} \tag{6}$$

Therefore, the minimum transfer effort for vehicle-slot pair (i,j) is

$$J_{ij}^{\min}=\Delta x_{ij}^T W^{-1}(T_p)\Delta x_{ij}, \qquad \Delta x_{ij}=x_{f,j}-e^{AT_p}x_i^0 \tag{7}$$

When the relative boundary velocities are zero, this becomes

$$J_{ij}^{\min}=\frac{12}{T_p^3}\| q_j-r_i^0 \|_2^2 \quad \text{for } w_i^0=w_{f,j}=0 \tag{8}$$

The T_p^{-3} law is important: the energy-feasibility margin deteriorates rapidly when the designer shortens the reconfiguration time. This creates a direct analytical coupling between deadline selection and maneuver effort rather than treating energy as an after-the-fact metric.

2.3. State-of-charge-weighted constrained assignment

Because vehicles do not necessarily start with equal mass or state of charge, the assignment objective weights the analytical effort by an induced-power-inspired mass factor and available battery fraction:

$$C_{ij}=\frac{(m_i/\bar{m})^{3/2}}{\max(\mathrm{SOC}_i,\epsilon_s)}J_{ij}^{\min} \tag{9}$$

where $\bar{m}$ is the fleet-mean mass and ε prevents division by a vanishing state of charge. The discrete optimization is

$$\pi^\star=\arg\min_{\pi\in\mathcal{P}_N}\sum_{i=1}^{N}C_{i,\pi(i)} \tag{10}$$

subject to individual maneuver-budget and pairwise-separation feasibility:

$$J_{i,\pi(i)}^{\min}\le\bar{J}_i, \qquad \min_{\tau\in[0,T_p]}\| r_i^\star(\tau)-r_j^\star(\tau)\|_2\ge d_{\text{safe}} \tag{11}$$

For $N = 6$, all $N!$ permutations are evaluated, so the reported solution is globally optimal within the stated discrete model and constraints. The same cost matrix can be passed to a linear-assignment or mixed-integer solver for larger fleets.

2.4. Minimum-energy predefined-time boundary trajectory

For the selected permutation, the boundary solution is a cubic polynomial,

$$r_i^\star(\tau)=a_{0i}+a_{1i}\tau+a_{2i}\tau^2+a_{3i}\tau^3 \tag{12}$$

with coefficients

$$a_{0i}=r_i^0,\ a_{1i}=w_i^0,\ a_{2i}=3\Delta r_i/T_p^2-2w_i^0/T_p,\ a_{3i}=-2\Delta r_i/T_p^3+w_i^0/T_p^2 \tag{13}$$

where D_i = $q_{\rho(i)}$ - r_i^0. Its relative velocity and acceleration are

$$w_i^\star=a_{1i}+2a_{2i}\tau+3a_{3i}\tau^2, \qquad a_i^\star=2a_{2i}+6a_{3i}\tau \tag{14}$$

The trajectory reaches the assigned final slot and zero relative velocity exactly at $t_s + T_p$ in the nominal boundary model.

2.5. Receding minimum-energy terminal correction

A key change from a conventional trajectory tracker is that the remaining tracking error is treated as a new finite-horizon steering problem. Define

$$e_i = r_i - r_i^\star, \qquad \dot{e}_i = w_i - w_i^\star, \qquad \xi_i = [e_i^T \ \dot{e}_i^T]^T \tag{15}$$

and the remaining time

$$t_r = t_s + T_p - t, \qquad 0 < t_r \le T_p \tag{16}$$

For the double-integrator error dynamics, the minimum-energy correction that drives the current error state to zero at the deadline is

$$\delta u_i^{\mathrm{ME}} = -B^T e^{A^T t_r} W^{-1}(t_r) e^{A t_r} \xi_i \tag{17}$$

Substitution of the closed-form Gramian gives

$$\delta u_i^{\mathrm{ME}} = -\frac{6}{t_r^2} e_i - \frac{4}{t_r} \dot{e}_i \tag{18}$$

Thus the position- and velocity-error gains are not selected independently of the deadline; they increase according to the physically meaningful remaining-time horizon. In code, the last 0.30 s is regularized to avoid numerical blow-up under sampled implementation and actuator limits, while a stabilizing feedback term remains active.

2.6. Effective-disturbance observer and robust tracking command

The unknown control-effectiveness deviation can be written as part of an effective disturbance,

$$d_i^{\mathrm{eff}} = (\beta_i - 1)u_i + d_i, \qquad y_{d,i} = a_i^{\mathrm{meas}} - (u_i - c_d w_i) \tag{19}$$

where a_i^{meas} is an acceleration estimate obtainable from an inertial/state estimator. A first-order bounded observer is used:

$$\dot{\hat{d}}_i = \lambda_d \, \mathrm{sat}_{\bar{d}_h}(y_{d,i} - \hat{d}_i) \tag{20}$$

With the composite error

$$z_i = \dot{e}_i + \lambda_e e_i \tag{21}$$

the pre-safety command is

$$u_i^0 = a_L + a_i^\star + \delta u_i^{\mathrm{ME}} - K_e e_i - K_v \dot{e}_i - \hat{d}_i - k_r \tanh(z_i / \varepsilon) \tag{22}$$

where the feedback gains and smoothing parameter are positive, and the hyperbolic tangent prevents chattering. The terminal correction and fixed feedback are complementary: the former explicitly preserves deadline recoverability, while the latter reduces transient sensitivity when the remaining time is still large.

2.7. Robust high-order control-barrier safety projection

Pairwise separation is expressed as

$$h_{ij} = \| p_i - p_j \|_2^2 - d_{\text{safe}}^2 \tag{23}$$

For a relative-degree-two barrier,

$$\psi_{1,ij} = \dot{h}_{ij} + \alpha_1 h_{ij} = 2 r_{ij}^T v_{ij} + \alpha_1 h_{ij} \tag{24}$$

and the robust second-order condition yields the linear acceleration inequality

$$2 r_{ij}^T (u_i - u_j) \geq b_{ij} = -2 \| v_{ij} \|^2 - 2(\alpha_1 + \alpha_2) r_{ij}^T v_{ij} - \alpha_1 \alpha_2 h_{ij} + 4 \| r_{ij} \| \bar{d} \tag{25}$$

where $\bar{d}$ bounds each vehicle's acceleration disturbance. Stacking all commanded accelerations into$u$ each violated pairwise half-space is corrected by the Euclidean minimum-norm projection

$$u \leftarrow u + \frac{[b_k - A_k u]_+}{\| A_k \|_2^2} A_k^T \tag{26}$$

The projection is applied sequentially for a small number of sweeps and only when a barrier inequality is violated. The final per-UAV command is projected to the admissible acceleration ball:

$$u_i = \Pi_{\|u\| \leq a_{\max}} (u_i^0) \tag{27}$$

2.8. Stability and optimality properties

Proposition 1. Equation (7) is the minimum squared-acceleration cost for the finite-horizon linear boundary problem, and (18) is the corresponding receding minimum-energy terminal control for the instantaneous tracking-error state. The result follows from the standard controllability-Gramian solution of the minimum-energy transfer problem.

Proposition 2. For $N = 6$, the assignment returned by exhaustive enumeration is globally optimal over the feasible permutation set defined by (11). This claim is discrete and exact; it does not depend on a heuristic optimizer.

Proposition 3. When the actuator projection is inactive, the HOCBF inequalities are feasible, and the observer error is bounded, the tracking dynamics are input-to-state practically stable with respect to the residual effective disturbance. A quadratic function

$$V_i = \frac{1}{2} \xi_i^T P \xi_i, \qquad P = P^T > 0 \tag{28}$$

can be selected for the regularized closed-loop error dynamics so that

$$\dot{V}_i \leq -\lambda_Q \| \xi_i \|^2 + c_1 \| \xi_i \| \| d_i^{\text{eff}} - \hat{d}_i \| \tag{29}$$

for suitable positive constants. Hence the tracking error enters a neighborhood proportional to the disturbance-estimation error. In the nominal observer-perfect case, the terminal correction drives the error to zero at the selected terminal time.

2.9. Propulsion-energy evaluation

The analytical assignment constraint uses squared acceleration because it permits a closed-form optimal transfer. Electrical/propulsion energy is evaluated independently. The required thrust magnitude is approximated by

$$F_i = m_i \left\| u_i + g e_3 \right\|_2 \tag{30}$$

and the multirotor power model is

$$P_i = P_0 + \frac{F_i^{3/2}}{\eta\sqrt{2\rho A_R}} + \frac{1}{2}\rho C_D A_f \| v_i \|_2^3 \tag{31}$$

This model follows the structure of validated multirotor energy models [22]–[27]. Incremental maneuver energy above hover is

$$E_i^+ = \int_{t_s}^{t_s+T_p} \max(P_i - P_{h,i}, 0)dt \tag{32}$$

This definition prevents the common hover component from masking differences between reconfiguration strategies.

2.10. Evaluation metrics and pseudocode

The primary metrics are

$$e_{\mathrm{RMS}}(t) = \sqrt{\frac{1}{N}\sum_{i=1}^{N} \| r_i - r_i^\star \|_2^2}, \qquad e_T = e_{\mathrm{final}}(t_s + T_p) \tag{33}$$

Separation and saturation are defined by

$$d_{\min} = \min_{t \geq t_s, i<j} \| p_i - p_j \|_2, \qquad \gamma_{\mathrm{sat}} = \frac{1}{NK}\sum_{k,i} \mathbf{1}_{\{\|u_i(k)\| \geq a_{\max}\}} 100\% \tag{34}$$

The practical completion criterion is final-formation RMSE below 0.12 m for at least 0.5 s.

Algorithm 1 - One reconfiguration cycle

Input: current follower states, target slots, masses, states of charge, maneuver-energy budgets, T_p, d_{safe}, and observer state.

(1) Compute J_{ij}^{min} and the SOC-weighted assignment costs.

(2) Enumerate/solve the assignment and reject budget/separation-infeasible candidates.

(3) At t_s, store the relative initial states and generate cubic boundary references.

(4) At each sample, update the remaining time and minimum-energy terminal correction.

(5) Update the effective-disturbance observer.

(6) Form the robust tracking command.

(7) Project violated HOCBF half-spaces.

(8) Apply the acceleration limit.

(9) Propagate the plant and update power, RMSE, separation, and energy metrics.

(10) Repeat until the maneuver is complete.

3. Simulation, Evaluation, and Discussion

3.1. Compound-uncertainty setup and fairness protocol

Six F450-class followers are simulated for 30 s with a 0.05 s sample period. Reconfiguration starts at t_s = 10 s and the nominal predefined duration is T_p = 8 s. The masses are [1.18, 1.32, 1.24, 1.38, 1.21, 1.29] kg and the initial state-of-charge fractions are

[0.92, 0.72, 0.86, 0.66, 0.80, 0.70]. The minimum separation is 1.75 m and the outer-loop acceleration limit is 6 m/s². The leader follows a smooth three-dimensional trajectory whose altitude is centered at 20 m.

The reported comparative evaluation focuses on the compound-uncertainty case, which combines stronger wind, heterogeneous control-effectiveness factors [0.93, 0.88, 0.98, 0.86, 0.95, 0.90], stochastic acceleration, and a localized opposing gust on a neighboring pair. Every compared method uses the same initial state, physical parameters, disturbance realization, and actuator limit. The common baseline gains are fixed before the test, and no method-specific gain retuning is used within the four-method comparison.

The four methods are: direct predefined-time mapping; energy-assigned predefined-time tracking; safe energy assignment with disturbance observation; and the full proposed method with receding terminal correction plus safety projection.

Table 1. Main simulation parameters

Parameter	Value	Unit	Role
Number of followers	6	-	Swarm size
Sampling period	0.05	s	20 Hz control loop
Reconfiguration start	10	s	Shape-switch time
Predefined duration	8	s	Mission deadline
Minimum separation	1.75	m	Safety constraint
Acceleration limit	6.0	m/s²	Outer-loop actuator bound
Disturbance bound for HOCBF	0.90	m/s²	Robust safety margin
Rotor radius	0.127	m	Propulsion-energy model
Air density	1.225	kg/m³	Standard atmosphere

3.2. Assignment result and energy feasibility

Table 2. Direct and proposed assignments

UAV	SOC	Mass (kg)	Direct slot	Proposed slot	J_{direct}	$J_{proposed}$	Budget
1	0.92	1.18	1	5	1.8984	0.1172	0.5661
2	0.72	1.32	2	4	0.6362	0.0302	0.5313
3	0.86	1.24	3	3	0.0302	0.0302	0.5556
4	0.66	1.38	4	2	0.9609	0.1172	0.5208
5	0.80	1.21	5	1	1.2857	0.4922	0.5452
6	0.70	1.29	6	6	0.4922	0.4922	0.5278

The direct mapping violates four of six maneuver budgets. The proposed permutation is [5, 4, 3, 2, 1, 6] in one-based slot numbering and satisfies all six budgets. Total reference effort decreases from 5.3036 to 1.2791, a 75.9% reduction. This improvement occurs before any feedback gain or disturbance compensation is applied.

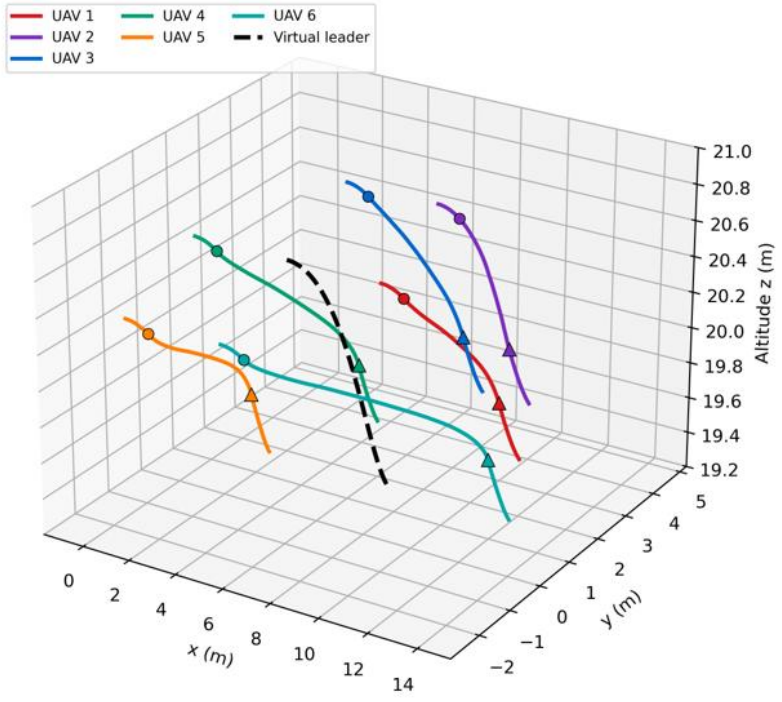


Figure 1. 3D formation reconfiguration under compound uncertainty

Quantitatively, all six followers complete the reconfiguration before the 8 s deadline; the proposed run settles in 7.05 s and retains a minimum pairwise separation of 1.997 m. This corresponds to an 11.9% deadline margin and a 14.1% separation margin relative to the 1.75 m threshold, with 0% acceleration saturation.

3.3. Tracking and deadline accuracy

Table 3. Compound-uncertainty comparison

Method	Tracking RMSE (m)	Post-deadline RMSE (m)	Deadline error (m)	Settling (s)	Incremental energy (J)	Min. separation (m)	Saturation (%)
Direct predefined-time	0.05437	0.03519	0.01654	7.35	65.49	0.225	0.00
Energy-assigned predefined-time	0.05384	0.03519	0.01650	7.00	60.24	1.972	0.00
Safe assigned + DOB	0.00621	0.00357	0.00415	7.05	55.48	1.997	0.00
Proposed EBPT-HOCBF	0.00529	0.00346	0.00176	7.05	55.16	1.997	0.00

The proposed method obtains 0.00529 m formation-reference RMSE and 0.00176 m error exactly at the 8 s deadline. Relative to direct predefined-time mapping, the RMSE reduction is 90.3% and the post-deadline RMSE reduction is 90.2%. Compared with the safe-assigned observer baseline, the proposed terminal correction reduces the deadline error from 0.00415 m to 0.00176 m while slightly reducing control effort and energy. No method saturates in this scenario, so the result is not produced by allowing the proposed controller to use a larger actuator envelope.

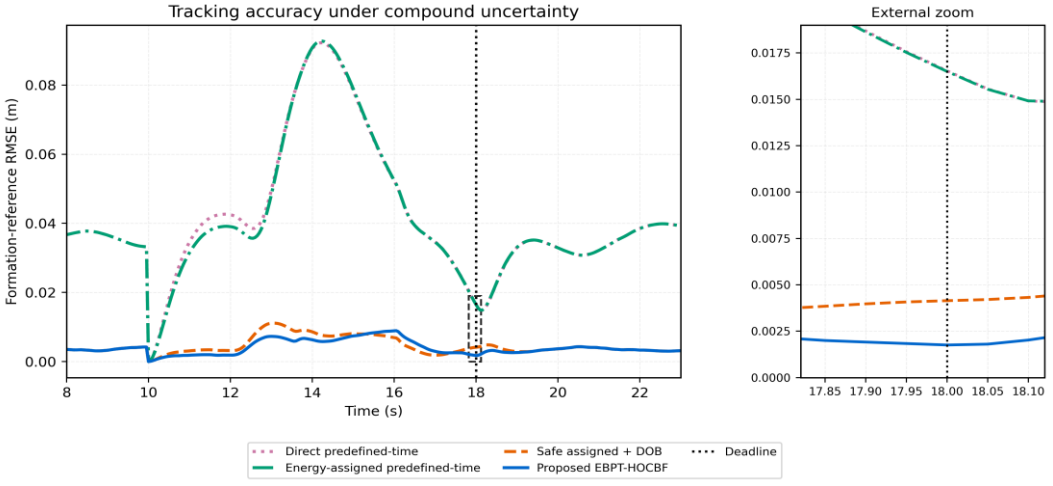


Figure 2. Formation-reference RMSE near the deadline

The proposed controller attains a formation-reference RMSE of 0.00529 m, compared with 0.00621 m for Safe assigned + DOB and 0.05437 m for direct predefined-time mapping. This corresponds to a 90.3% RMSE reduction relative to the direct baseline, while the external zoom confirms that the proposed curve remains lower around the deadline. The 14.8% reduction relative to Safe assigned + DOB isolates the incremental accuracy benefit of the receding terminal correction.

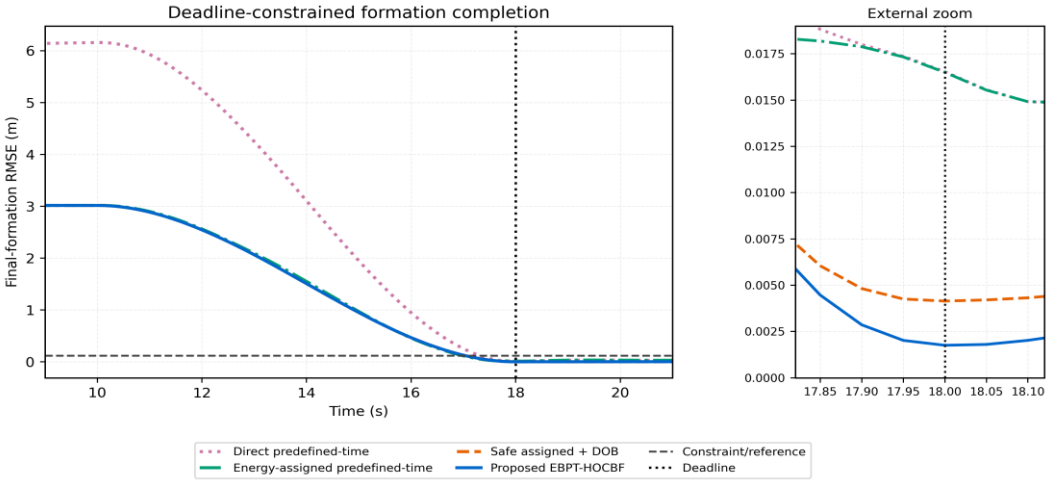


Figure 3. Final-formation error at the deadline

At the predefined deadline, the proposed error is 0.00176 m versus 0.00415 m for Safe assigned + DOB, a 57.6% reduction. The settling time is 7.05 s, leaving approximately 0.95 s of deadline margin without increasing the acceleration limit. The 1.76 mm deadline error is only 1.47% of the 0.12 m completion threshold.

3.4. Safety, control effort, and propulsion energy

The direct mapping creates severe geometric conflict: minimum separation is only 0.225 m. Energy-aware assignment alone increases it to 1.972 m, while both disturbance-observer methods maintain approximately 1.997 m. The proposed barrier

supervisor activates only two pairwise projections in the compound run and does not change the saturation ratio, confirming that the nominal assignment carries most of the geometric safety burden while the barrier layer remains available for local correction.

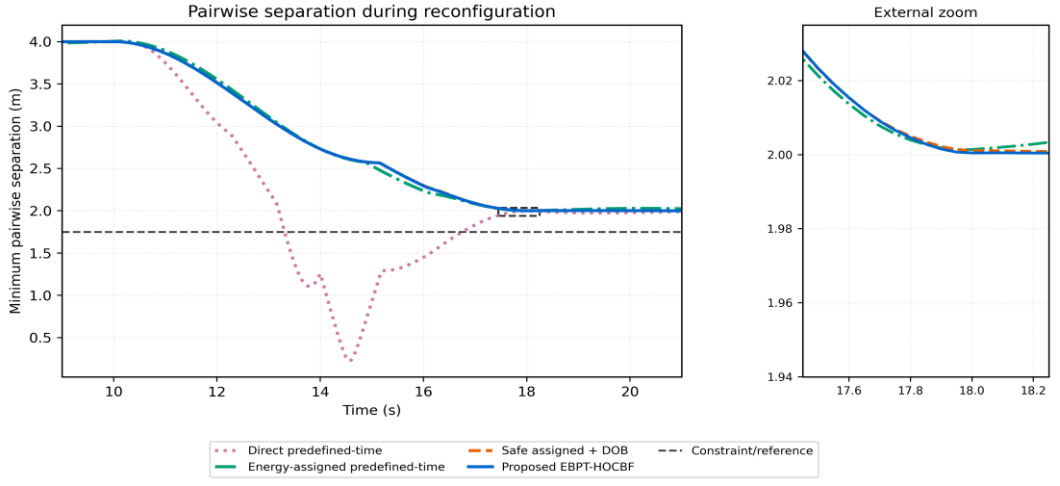


Figure 4. Minimum pairwise separation

The proposed and Safe + DOB methods maintain a minimum separation of approximately 1.997 m, providing a 0.247 m margin above the 1.75 m safety threshold; the energy-assigned baseline reaches 1.972 m, whereas direct mapping collapses to 0.225 m. The selected zoom therefore focuses only on the feasible methods near their closest approach. Thus, the proposed minimum separation is 14.1% above the safety threshold, whereas direct mapping is 87.1% below it.

The cumulative commanded-acceleration effort of the full method is 37.28 compared with 47.49 for direct mapping. The independently evaluated incremental propulsion energy decreases from 65.49 J to 55.16 J, corresponding to a 15.8% reduction. The reduction relative to the energy-assigned baseline is 8.4%, which isolates the benefit of disturbance estimation and the terminal-recovery law after the discrete assignment has already been improved.

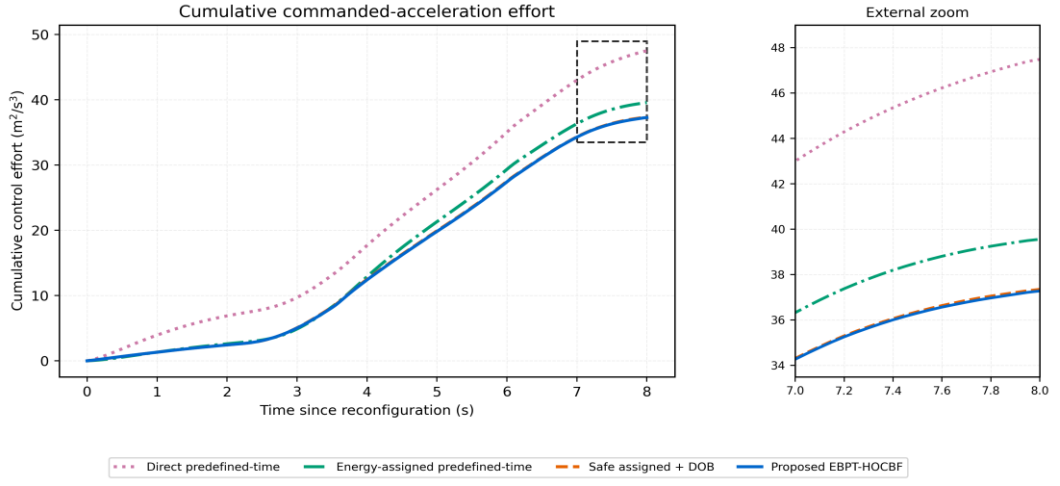


Figure 5. Cumulative control effort

The proposed cumulative control effort is 37.28, compared with 47.49 for direct mapping and 39.56 for energy-assigned predefined-time control. Thus, the proposed method reduces control effort by 21.5% relative to the direct baseline and remains

slightly below the Safe + DOB case (37.35). It is also about 0.2% lower than Safe + DOB, showing that the accuracy gain is not obtained by increasing total acceleration effort.

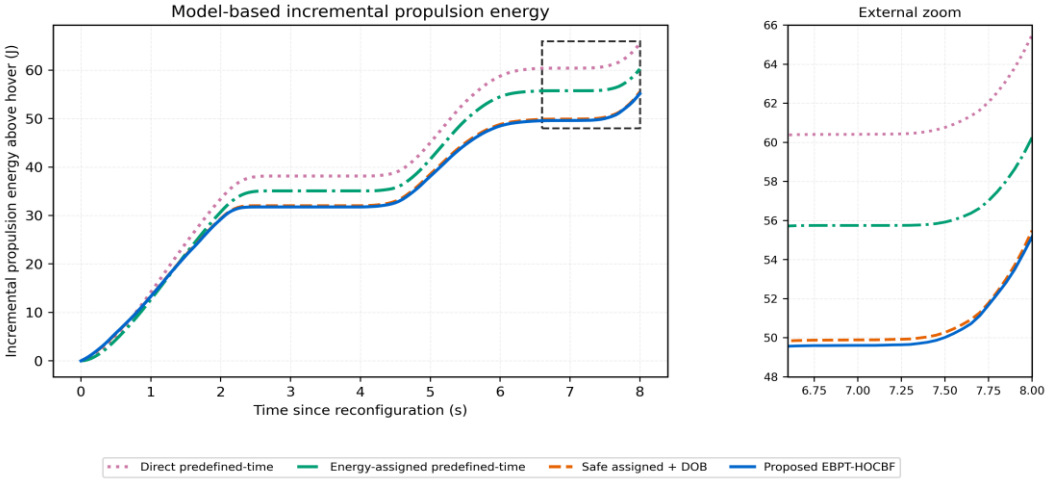


Figure 6. Incremental propulsion energy above hover

The proposed incremental propulsion energy is 55.16 J, compared with 65.49 J for direct mapping and 60.24 J for energy-assigned predefined-time control. The reductions are 15.8% and 8.4%, respectively, while the terminal zoom shows that the proposed curve remains marginally below Safe + DOB through the final interval. Relative to Safe + DOB (55.48 J), energy is 0.58% lower while deadline error is reduced by 57.6%.

3.5. Ablation study

The ablation uses one fixed common seed (121) for all configurations; Table 4 should therefore be interpreted by paired within-table differences rather than by comparing its absolute values with Table 3.

Table 4. Component ablation under the compound case

Configuration	Tracking RMSE	Post RMSE	Deadline error	Control effort	Incremental energy	Min. separation
Full proposed	0.00523	0.00338	0.00164	37.26	55.16	1.997
Without terminal correction / HOCBF projection	0.00611	0.00349	0.00383	37.33	55.49	1.997
Without DOB and safety projection	0.05379	0.03519	0.01640	39.55	60.37	1.973
Without energy/safety assignment	0.05432	0.03518	0.01644	47.44	65.60	0.220

Removing the terminal/safety layer increases tracking RMSE from 0.00523 to 0.00611 and more than doubles deadline error from 0.00164 to 0.00383 m. Removing the disturbance observer increases RMSE by roughly one order of magnitude. Removing the energy/safety assignment leaves the deadline tracker active but collapses minimum separation to approximately 0.22 m and increases both control effort and propulsion energy. The ablation therefore separates the contributions instead of attributing all improvement to one tuned feedback gain.

3.6. Thirty-trial Monte Carlo robustness

Table 5. Thirty common-seed trials under compound uncertainty (mean ± standard deviation)

Method	Tracking RMSE (m)	Post RMSE (m)	Mean deadline error (m)	Deadline success (%)	Worst min. separation (m)	Mean incremental energy (J)
Direct predefined-time	0.05437 ± 0.00005	0.03513 ± 0.00007	0.01651	100	0.220	66.06
Energy-assigned predefined-time	0.05384 ± 0.00005	0.03514 ± 0.00007	0.01647	100	1.971	60.87
Safe assigned + DOB	0.00615 ± 0.00005	0.00358 ± 0.00004	0.00403	100	1.996	55.97
Proposed EBPT-HOCBF	0.00527 ± 0.00004	0.00347 ± 0.00005	0.00173	100	1.996	55.69

The proposed method maintains 100% deadline success over seeds 101–130. Its mean post-deadline RMSE is 0.00347 m with standard deviation 0.00005 m, and the worst observed minimum separation is 1.996 m. The common-seed design ensures each method sees the same random realization in each trial.



Figure 7. Paired Monte Carlo improvement over Safe + DOB.

Across all 30 paired seeds, the proposed method improves on Safe+DOB in every realization. The mean paired differences (Proposed - Safe+DOB) are -0.880 ± 0.008 mm for tracking RMSE, -2.298 ± 0.017 mm for deadline error, and -0.282 ± 0.012 J for incremental energy, where the intervals are 95% confidence half-widths. The consistent negative sign in 30/30 trials shows that the gain is not seed-specific.

3.7. Sensitivity to the predefined time

All deadline cases use the same compound-disturbance seed (131), and the nominal 8 s assignment is held fixed so that the comparison isolates sensitivity to the selected deadline.

Table 6. Deadline sensitivity of the proposed method

T_p (s)	Tracking RMSE	Deadline error	Settling (s)	Control effort	Incremental energy (J)	Min. separation (m)
6	0.00469	0.00263	5.30	30.80	52.13	1.995
7	0.00522	0.00086	6.15	36.59	52.05	1.997
8	0.00524	0.00171	7.05	37.30	56.29	1.997
9	0.00526	0.00063	7.95	36.60	73.70	1.997
10	0.00520	0.00158	8.85	36.16	81.82	1.997

The controller reaches the 0.12 m completion band before each tested deadline from T_p = 6 to 10 s. Tracking RMSE remains below 0.0053 m. The non-monotonic propulsion-energy trend is expected because the reported quantity includes the time-varying wind response over the entire reconfiguration interval, whereas the analytical reference-effort term follows the T_p^{-3} law. This distinction is why the paper reports both the analytical maneuver index and the propulsion-energy estimate.

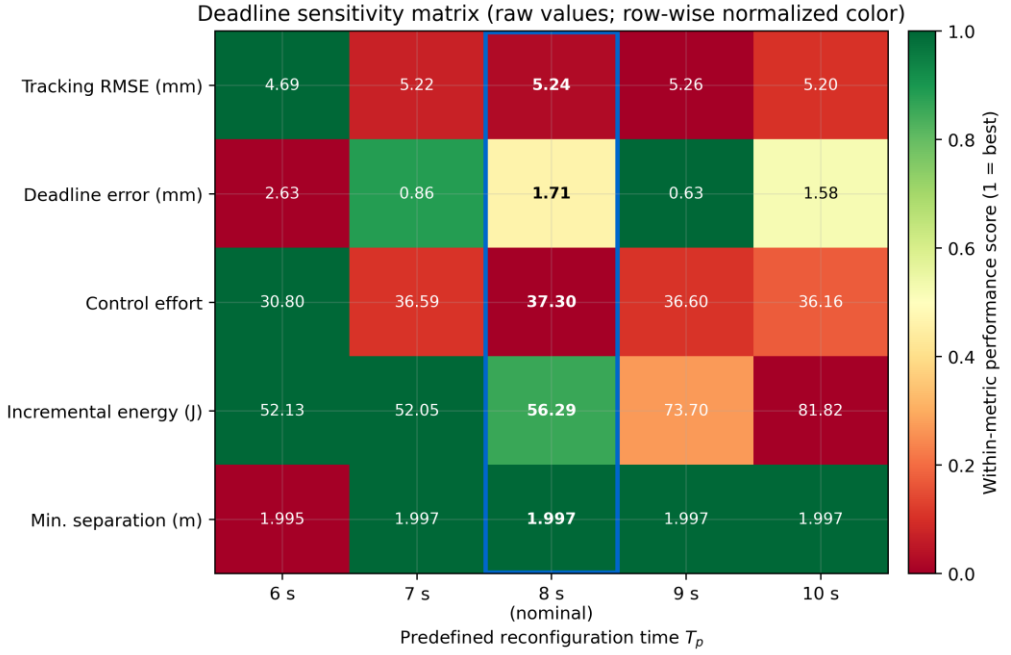


Figure 8. Deadline-sensitivity matrix

Across T_p = 6-10 s, tracking RMSE remains within 4.69-5.26 mm and minimum separation within 1.995-1.997 m. The nominal T_p = 8 s case gives 5.24 mm tracking RMSE, 1.71 mm deadline error, 37.30 control effort, and 56.29 J incremental energy. The matrix also shows that T_p = 7 s uses less energy (52.05 J), whereas T_p = 9 s gives the smallest deadline error (0.63 mm); therefore, no single deadline minimizes all metrics. The result characterizes the selected deadline as a multi-objective mission-design variable rather than a parameter with one universal optimum.

3.8. Discussion and synthesis

The numerical evidence identifies distinct roles for the proposed architecture. The Gramian-based assignment removes energetically expensive and geometrically unsafe mappings before flight, thereby reducing reference effort and avoiding unnecessary safety intervention. Effective-disturbance observation suppresses model mismatch and wind-induced acceleration error, while the receding terminal correction directly restores the finite-horizon boundary condition from the instantaneous tracking state. The HOCBF layer then acts as a minimally invasive safety supervisor. Because all compared methods share the same initial states, disturbance realizations, actuator limits, and baseline gains, the improvements are attributable to these structural mechanisms rather than method-specific retuning. The paired Monte Carlo results further show that the terminal-correction benefit is systematic across random realizations, and the deadline-sensitivity study confirms that the selected reconfiguration time is a genuine mission-design variable that trades terminal accuracy, control effort, and propulsion energy.

4. Conclusion

An energy-constrained predefined-time formation-reconfiguration framework for heterogeneous UAV swarms has been established by coupling deadline-dependent Gramian assignment, receding minimum-energy terminal recovery, effective-disturbance observation, and HOCBF safety. The principal result is the use of one finite-horizon energy metric across both the discrete and continuous layers: the mission deadline therefore enters the slot-allocation problem and the online correction law in a consistent analytical form. In the compound-uncertainty case, the method achieves 5.29 mm tracking RMSE, 1.76 mm deadline error, 1.997 m minimum separation, and zero acceleration saturation. Relative to direct predefined-time mapping, reference maneuver effort decreases by 75.9%, tracking RMSE by 90.3%, and incremental propulsion energy by 15.8%. Thirty paired common-seed trials retain 100% deadline success, while the ablation study confirms that energy/safety assignment governs feasibility and effort and that disturbance observation with receding terminal correction provides the dominant accuracy gain. These results support the proposed Gramian-coupled architecture as an analytically transparent and computationally compact approach to energy-aware, deadline-critical swarm reconfiguration.

Declaration of Conflicting Interests

The author declares no potential conflicts of interest with respect to the research, authorship, and publication of this article.

Funding

The author received no financial support for the research, authorship, and publication of this article.

References

[1] C. Yu, J. Liu, P. Xie, and W. Xie, “A Comprehensive Review of UAV Formation Control from a Mission-Driven Perspective,” Drones, vol. 10, no. 4, art. 278, 2026. https://doi.org/10.3390/drones10040278

[2] F. Sun, J. Su, W. Zhu, Z.-H. Guan, and J. Kurths, “Predefined-time formation control of UAV swarm under spatiotemporal constraints,” ISA Transactions, vol. 170, pp. 187–199, 2026. https://doi.org/10.1016/j.isatra.2026.01.025

[3] W. Yang, J. Liu, Y. Ma, H.-K. Lam, and J. Yu, “Predefined-time distributed optimal formation control for constrained UAV-UGV systems,” ISA Transactions, vol. 176, pp. 298–308, 2026. https://doi.org/10.1016/j.isatra.2026.06.008

[4] Q. Lin, Y. Liu, Z.-G. Wu, and W. Gui, “Predefined-Time Formation Control for Various Heterogeneous Autonomous Systems,” IEEE Transactions on Intelligent Transportation Systems, vol. 27, no. 5, pp. 5467–5476, 2026. https://doi.org/10.1109/TITS.2026.3654998

[5] J. Su and Y. Song, "Prescribed-Time Formation Control for Multi-Agent Systems With Uncertain Nonlinear Dynamics and Non-Vanishing Random Disturbances," IEEE/CAA Journal of Automatica Sinica, vol. 13, no. 3, pp. 586–596, 2026. https://doi.org/10.1109/JAS.2026.125714

[6] Y. Chen, B. Hao, F. Niu, Z. Wei, X. Nian, and X. Dai, "Prescribed-time bearing-based time-varying formation control for multi-agent system," ISA Transactions, vol. 175, pp. 538–549, 2026. https://doi.org/10.1016/j.isatra.2026.04.036

[7] T. Hou, W. Bi, Z. Huang, P. Yang, and A. Zhang, "Time-varying formation tracking for multi-agent systems based on prescribed-time control," Proc. IMechE Part I: Journal of Systems and Control Engineering, vol. 239, no. 6, pp. 1093–1106, 2025. https://doi.org/10.1177/09596518241309128

[8] P. De Villeros, J. D. Sánchez-Torres, M. Defoort, M. Djemaï, and A. Loukianov, "Predefined-Time Formation Control for Multiagent Systems-Based on Distributed Optimization," IEEE Transactions on Cybernetics, vol. 53, no. 12, pp. 7980–7988, 2023. https://doi.org/10.1109/TCYB.2023.3264541

[9] P. De Villeros, R. Aldana-López, J. D. Sánchez-Torres, M. Defoort, M. Djemaï, and A. Loukianov, "Distributed predefined-time optimization in formation control under switching topologies," IFAC-PapersOnLine, vol. 56, no. 2, pp. 43–48, 2023. https://doi.org/10.1016/j.ifacol.2023.10.1389

[10] J. Wang, X. Ding, C. Wang, L. Liang, and H. Hu, "Affine formation control for multi-agent systems with prescribed convergence time," Journal of the Franklin Institute, vol. 358, no. 14, pp. 7055–7072, 2021. https://doi.org/10.1016/j.jfranklin.2021.07.019

[11] T.-F. Ding, M.-F. Ge, C. Xiong, Z.-W. Liu, and G. Ling, "Prescribed-time formation tracking of second-order multi-agent networks with directed graphs," Automatica, vol. 152, art. 110997, 2023. https://doi.org/10.1016/j.automatica.2023.110997

[12] R. Aldana-López, D. Gómez-Gutiérrez, R. Aragüés, and C. Sagüés, "Dynamic consensus with prescribed convergence time for multileader formation tracking," IEEE Control Systems Letters, vol. 6, pp. 3014–3019, 2022. https://doi.org/10.1109/LCSYS.2022.3181784

[13] X. Li, Y. Zhu, X. Zhao, and J. Lu, "Bearing-based prescribed time formation tracking for second-order multi-agent systems," IEEE Transactions on Circuits and Systems II: Express Briefs, vol. 69, no. 7, pp. 3259–3263, 2022. https://doi.org/10.1109/TCSII.2022.3141735

[14] B. Li, W. Gong, B. Xiao, and Y. Yang, "Distributed prescribed-time leader-following formation control for second-order multi-agent systems with mismatched disturbances," International Journal of Robust and Nonlinear Control, vol. 33, no. 16, pp. 9781–9803, 2023. https://doi.org/10.1002/rnc.6878

[15] Y. Jiang, Z. Liu, and Z. Chen, "Prescribed-time distributed formation control for a class of nonlinear multi-agent systems subject to internal uncertainties and external disturbances," Nonlinear Dynamics, vol. 111, pp. 1643–1655, 2023. https://doi.org/10.1007/s11071-022-07909-2

[16] B. Li, Z. Guo, C. Hu, S. Zhu, and S. Wen, "Safe formation control of uncertain multiagent systems from a Bayesian perspective," IEEE Transactions on Automatic Control, vol. 70, no. 3, pp. 1929–1934, 2025. https://doi.org/10.1109/TAC.2024.3470928

[17] Y. Lu, K. Zhang, and B. Jiang, "Fully actuated system approach based prescribed-time fault-tolerant formation control for unmanned helicopters under fixed and switching topologies," IEEE Transactions on Circuits and Systems I: Regular Papers, vol. 71, no. 11, pp. 5249–5260, 2024. https://doi.org/10.1109/TCSI.2024.3399779

[18] Y. Li, X. Zheng, and K. Li, "Prescribed-Time Adaptive Intelligent Formation Controller for Nonlinear Multiagent Systems Based on Time-Domain Mapping," IEEE Transactions on Artificial Intelligence, vol. 5, no. 4, pp. 1778–1790, 2024. https://doi.org/10.1109/TAI.2023.3299439

[19] X. Gong, M. V. Basin, Z. Feng, T. Huang, and Y. Cui, "Resilient time-varying formation-tracking of multi-UAV systems against composite attacks: A two-layered framework," IEEE/CAA Journal of Automatica Sinica, vol. 10, no. 4, pp. 969–984, 2023. https://doi.org/10.1109/JAS.2023.123339

[20] C. Gao, J. Ma, T. Li, and Y. Shen, "Hybrid swarm intelligent algorithm for multi-UAV formation reconfiguration," Complex & Intelligent Systems, vol. 9, pp. 1929–1962, 2023. https://doi.org/10.1007/s40747-022-00891-7

[21] J. Liao, X. Gao, S. Yan, S. Zhou, D. Wang, and Y. Kang, "Formation reconfiguration control of UAV swarm based on MPC-PIO," Journal of Beijing University of Aeronautics and Astronautics, vol. 50, no. 5, pp. 1541–1550, 2024. https://doi.org/10.13700/j.bh.1001-5965.2022.0398

[22] H. Gong, B. Huang, B. Jia, and H. Dai, "Modeling Power Consumptions for Multirotor UAVs," IEEE Transactions on Aerospace and Electronic Systems, vol. 59, no. 6, pp. 7409–7422, 2023. https://doi.org/10.1109/TAES.2023.3288846

[23] M. Jacewicz, M. Żugaj, R. Głębocki, and P. Bibik, "Quadrotor Model for Energy Consumption Analysis," Energies, vol. 15, no. 19, art. 7136, 2022. https://doi.org/10.3390/en15197136

[24] H. Yan, Y. Chen, and S.-H. Yang, "New Energy Consumption Model for Rotary-Wing UAV Propulsion," IEEE Wireless Communications Letters, vol. 10, no. 9, pp. 2009–2012, 2021. https://doi.org/10.1109/LWC.2021.3090772

[25] Y. Zeng, J. Xu, and R. Zhang, "Energy Minimization for Wireless Communication With Rotary-Wing UAV," IEEE Transactions on Wireless Communications, vol. 18, no. 4, pp. 2329–2345, 2019. https://doi.org/10.1109/TWC.2019.2902559

[26] A. H. B. M. Tavares, S. Luiz, T. P. Nascimento, and A. M. N. Lima, "Trade-off between flight performance and energy consumption of a quadrotor," Mechatronics, vol. 108, art. 103316, 2025. https://doi.org/10.1016/j.mechatronics.2025.103316

[27] V. Honcharenko and V. Yesilevskyi, "An Analytical Model of Quadrotor Electrical Energy Consumption," Engineering, Technology & Applied Science Research, vol. 16, no. 2, pp. 33302–33309, 2026. https://doi.org/10.48084/etasr.15062

[28] G. Wen, C. L. P. Chen, J. Feng, and N. Zhou, "Optimized multi-agent formation control based on an identifier-actor-critic reinforcement learning algorithm," IEEE Transactions on Fuzzy Systems, vol. 26, no. 5, pp. 2719–2731, 2018. https://doi.org/10.1109/TFUZZ.2017.2787561

[29] Đ. V. Thanh, "Development of Stabilization and Control Algorithms for a Small-Scale Tri-Rotor UAV," Ph.D. Dissertation in Engineering, 2021.. https://hdl.handle.net/11742/74795

[30] Đ. C. Vu, "Design of an Adaptive Controller to Ensure Flight Safety for Small UAVs under Wind Disturbances," Ph.D. Dissertation in Engineering, Military Technical Academy, Hanoi, 2018.. https://sdh.mta.edu.vn/

[31] A. Karimoddini, H. Lin, B. M. Chen, and T. H. Lee, "Hybrid three-dimensional formation control for unmanned helicopters," Automatica, vol. 49, no. 2, pp. 424–433, 2013. https://doi.org/10.1016/j.automatica.2012.10.008

[32] R. Guardeño, M. J. López, and V. M. Sánchez, "MIMO PID Controller Tuning Method for Quadrotor Based on LQR/LQG Theory," Robotics, vol. 8, no. 2, art. 36, 2019. https://doi.org/10.3390/robotics8020036